

Use Authorization

In presenting this thesis in partial fulfillment of the requirements for an advanced degree at Idaho State University, I agree that the Library shall make it freely available for inspection. I further state that permission to download and/or print my thesis for scholarly purposes may be granted by the Dean of the Graduate School, Dean of my academic division, or by the University Librarian. It is understood that any copying or publication of this thesis for financial gain shall not be allowed without my written permission.

Signature_____

Date_____

A Computational Fluid Dynamics Analysis of Choked Flow through an Orifice

by

Eliel Suarez

A thesis

submitted in partial fulfillment

of the requirements for the degree of

Master of Science in the Department of Nuclear Engineering

Idaho State University

Spring 2018

Copyright 2017 Eliel Jose Suarez

Committee Approval Page

To the Graduate Faculty:

The members of the committee appointed to examine the thesis of ELIEL JOSE SUAREZ find it satisfactory and recommend that it be accepted.

Dr. Richard Schultz,

Major Advisor

Dr. Ken Bosworth,

Graduate Faculty Representative

Dr. Jay Kunze,

Committee Member

Acknowledgement Page

I would like to show gratitude for all those who made this thesis possible. Thank you Idaho State University for the necessary resources required to produce this thesis. Thank you Dr. Ken Bosworth and Dr. Jay Kunze for providing comments and showing professionalism during my thesis defense. A very special thank you to Dr. Richard Schultz for mentoring me and providing expertise and guidance for my research.

Table of Contents

List of Figures	vii
List of Tables	viii
List of Equations	ix
Thesis Abstract—Idaho State University (2018)	x
Section I: Introduction	1
Need	1
Objectives	2
Approach	2
Section II: Literature Review	3
Discussion and findings	3
Summary of literature review:	11
Section III: Description of Hardware and Instrumentation	12
Hardware	12
Instrumentation	15
Section IV: Hand calculations	18
Section V: COMSOL	19
COMSOL software description and computing specifications	19
Space dimension	22
Geometry	23
Material	23
Fluid flow interface	24
Turbulence model	25
Meshing	26
Study	28
Rarefied gas flow:	29
Post Processing Analysis	30
Section VI: COMSOL calculations	32
Section VII: Results	33
High Mach number Flow k- ϵ	33
Grid Convergence study	38

Section VIII: Conclusions and Observations	41
References	42
Appendices.....	44
Appendix A: Knudsen number calculation	44
Appendix B: COMSOL study procedure	45
Procedure for a High Mach Number Flow k- ϵ study:	45
Appendix C: Mass flow rate calculations	51
HMNF k- ϵ , 1/16-inch:	51
HMNF k- ϵ , 1/32-inch:	51
HMNF k- ϵ , 1/64-inch:	52
Appendix D: COMSOL convergence plots	53
Hmnf k- ϵ cases:	53
Appendix E: Maestas results	55

List of Figures

Figure 1. Basic flow patterns when the flow first approaches the choked condition.	4
Figure 2. Graph showing the relationship between C_d and t/d . Ward-Smith (1979)	8
Figure 3. Experimental apparatus used in Maestas (2015).	12
Figure 4. Experiment Hardware and Instrumentation.....	15
Figure 5. Instrumentation arrangement.....	16
Figure 6. COMSOL model builder tree.	21
Figure 7. COMSOL space dimension.	22
Figure 8. 2D geometry model.	23
Figure 9. Material contents.	24
Figure 10. COMSOL physics modules.	25
Figure 11. Predefined mesh size settings and statistics.	27
Figure 12. Coarse meshing. Full system meshing (left). Orifice meshing (right).	28
Figure 13. Post processing analysis steps.	31
Figure 14. Hmnf $k-\epsilon$, velocity profile, 1/16 inch.	34
Figure 15. Hmnf $k-\epsilon$, velocity profile, 1/32 inch.	34
Figure 16. Hmnf $k-\epsilon$, velocity profile, 1/64 inch.	35
Figure 17. Pressure profiles at the orifice: 1/16 inch (hmnf $k-\epsilon$).	36
Figure 18. Pressure profiles at the orifice: 1/32 inch (hmnf $k-\epsilon$).	36
Figure 19. Pressure profiles at the orifice: 1/64 inch (hmnf $k-\epsilon$).	37
Figure 20. Convergence plot, hmnf $k-\epsilon$. Coarse (higher), normal (middle), fine (lower).	39
Figure 21. Parameters.	46
Figure 22. Inlet (left) and Outlet (right) boundaries.	49
Figure 23. Average surface derivation expressions for a receiving vessel model.	50
Figure 24. 1/16-inch convergence plot (hmnf $k-\epsilon$).	53
Figure 25. 1/32-inch convergence plot (hmnf $k-\epsilon$).	53
Figure 26. 1/64-inch convergence plot (hmnf $k-\epsilon$).	54

List of Tables

Table 1. Critical Discharge Coefficients.....	7
Table 2. Major components of experimental apparatus used in Maestas (2015).....	13
Table 3. Instrumentation identification.....	16
Table 4. Hand calculation critical mass flow rate.....	18
Table 5. Computer and COMSOL specifications.	21
Table 6. Inlet and Outlet pressure cases.....	32
Table 7. Boundary conditions.	32
Table 8. Hmnf k- ϵ mass flow rates.	33
Table 9. Mesh size solution (1/32", hmnf k- ϵ).	40
Table 10. Maestas average mass flow rates.....	55

List of Equations

Equation 1, critical pressure ratio.	9
Equation 2, Standard Critical Mass Flow Rate with Discharge Coefficient.....	18
Equation 3, Knudsen Number.....	29
Equation 4, Knudsen Number alternative.....	29
Equation 5, Mass flow rate.	30
Equation 6, Percent change Formula.	32

Thesis Abstract—Idaho State University (2018)

A computational fluid dynamics (CFD) validation study was performed to study the feasibility of using the COMSOL Multiphysics software to calculate critical gas flow through flat-plate orifices with a constant bore diameter. Calculations were performed for three different circular orifice plates with the following diameters (inch): 1/16, 1/32, and 1/64 with orifice plate thickness-to-diameter ratios of 2, 4, and 8 respectively. Lastly, a CFD study was performed to calculate the thermodynamic state conditions in the downstream receiver vessel.

COMSOL calculations didn't calculate the correct critical mass flow rate, grid convergence studies demonstrated that the code didn't converge, and COMSOL was found to not have an appropriate turbulence model to calculate the behavior of jets at Mach numbers above 0.3 where compressibility effects are important. Therefore, COMSOL, in its present form, cannot be used to calculate the critical mass flow rate through orifices nor the conditions downstream of the orifices.

Section I: Introduction

There are different methods to measure flow rates. A common method is the critical flow orifice plate meter stemming from its simple structure and minimal measurement requirements. A critical flow orifice is easy and cheap to build and also requires only a few diagnostics.

Typically when an orifice plate is used to measure mass flow rates it is inserted in the flow passage and the resulting pressure drop through the orifice plate is used to calculate the mass flow rate. Critical orifice meters, on the other hand, only need the upstream pressure and temperature to determine the mass flow rate of the fluid as long as the downstream pressure is below the critical pressure. Critical or choked flow occurs when the fluid at the throat of the orifice is at the speed of sound (Mach 1). Thus, the sound waves, which are traveling pressure waves moving at the speed of sound, are unable to inform the regions upstream of the orifice the magnitude of the pressure downstream of the orifice.

Need

An Idaho State University graduate, Joe Maestas (Maestas, 2015) performed flow experiments using critical flow orifices to investigate the feasibility of using them to measure mass flow rates using nitrogen gas—to earn his M. Sc. thesis in mechanical engineering. To accomplish this objective, an experimental apparatus consisting of a nitrogen gas bottle coupled to a flange housing a critical flow orifice that exhausted the nitrogen gas into a receiver tank was constructed and used. By reducing the pressure in the receiver tank to a near zero condition critical flow was achieved through the orifice. Instrumentation capable of measuring the mass flow rate through each of four orifices was mounted while the downstream conditions in the receiver tank were monitored using a pressure transducer and thermocouple.

Of interest, in addition to the mass flow rates, is also the behavior of the nitrogen discharging into the receiver tank since the flow must transition from a critical flow condition to an equilibrium condition. Hence a COMSOL calculation of the flow in the receiver tank was proposed and is examined in this report.

Objectives

The main objectives for this thesis are as follows; first, use COMSOL software to perform a theoretical calculation predicting gas flow behavior through the critical orifice plates deployed by Mr. Maestas. Second, to perform validation calculations that not only predict the critical mass flow rates but also predict the downstream behavior in the receiver tank. Third and last, to evaluate whether or not COMSOL can be used to calculate the critical mass flow rate through pipes and/or experimental apparatus such as that used by Mr. Maestas.

Approach

Hand calculations were performed using guidance from the text: Zucker & Biblarz, 2002. Then, COMSOL community standard practices were used to construct a COMSOL model and perform calculations of the critical mass flow rates and the behavior in the receiver tank. Finally it was hoped that the COMSOL software could be validated by comparing the calculation to the data recorded by Maestas.

Section II: Literature Review

Discussion and findings

The literature review focused on whether comprehensive data are available that describe the flow field behavior in the vicinity of a critical flow orifice and the downstream region. To characterize an orifice used to measure critical flow an important variable is the orifice thickness (t) to bore diameter (D) ratio (t/D). The critical orifices used by Maestas (2015) had the following bore diameters: 1/16-inch, 1/32-inch, and 1/64-inch. Two 1/64-inch diameter orifices were used—one with a sharp-edged chamfered inlet and the other with a constant diameter 1/64-inch bore through the orifice plate. The thickness of these orifice plates were all 0.125-inch and thus the t/D ratios were: 2.0, 4.0, and 8.0 respectively for the orifice plates with a constant diameter bore through the orifice plate. For the 1/64-inch diameter orifice with a chamfered sharp-edge, the t/D was 2. Findings from the references are discussed and summarized.

Ward-Smith (1979) studied critical flow behavior through orifices from the perspective of separated and reattached flow. For a sharp-edged orifice separation will occur at the orifice leading edge. If the flow does not reattach, or is only marginally reattached—as shown in Figure 1a, then the discharge coefficient will vary according to the value of the critical pressure ratio (downstream pressure/upstream pressure = P_6/P_1). If the flow fully reattaches in the orifice and there is not a significant length beyond the attachment point, then choking occurs; orifices with such characteristics have t/D ratios between δ and ϵ —see Figure 1b and will exhibit the desired choked flow characteristic where the flow will not vary as the P_6/P_1 ratio is decreased. Orifices with t/D ratios greater than ϵ (see Figure 1c) are governed by Fanno flow where choking is achieved at the exit plane of the orifice. Ward-Smith, 1979 concluded that:

“Theoretical and experimental evidence has been used to demonstrate that, for sharp-edged orifices, there exists a range of values of t/D , for which, within experimental limits, the critical discharge coefficient is independent of Reynolds number and t/D . This result has important practical consequences. The range is determined by the limit $\delta < t/D < \varepsilon$. Theory indicates that the magnitude of δ is determined solely by the sharpness or otherwise of the leading edge of the orifice. The actual magnitude of δ has not been precisely determined, but, for the orifices with nominally sharp edges that have been investigated, the experimental results analyzed give results varying from $\delta \sim 0.3$ to $\delta \sim 1$. Theory shows that the upper limit $t/D = \varepsilon$ is a function of Reynolds number and relative roughness. For the rough bore used in the present experiments a value of $\varepsilon = 7$ was determined; other results where a smoother bore was used are consistent with $\varepsilon \sim 10$.”

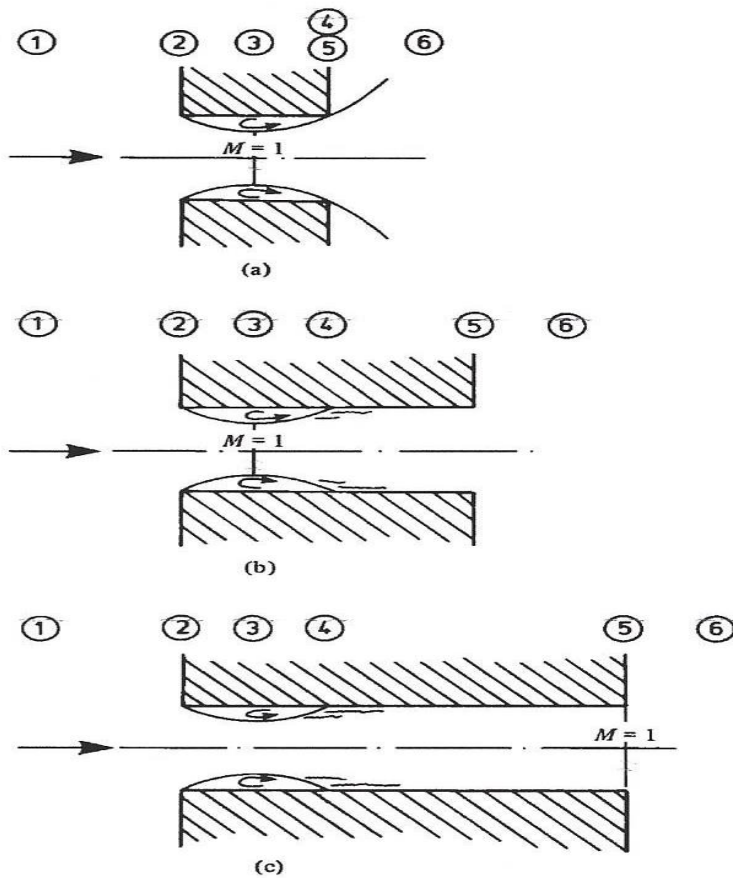


Fig. 2. Basic flow patterns when the flow first approaches the choked condition
 (a) Marginally reattached flow; $0 < t/d < \delta$
 (b) Fully reattached flow; $\delta < t/d < \varepsilon$
 (c) Fully reattached flow; $t/d > \varepsilon$

Figure 1. Basic flow patterns when the flow first approaches the choked condition.

Ward-Smith (1979) also had several useful observations regarding the shock behavior downstream of the choking plane for the orifice geometries shown in Figures 1a and 1b, i.e., the reduction of the back pressure, P_6 , below that corresponding to Figures 1a and 1b: "...results initially in the formation of a weak normal shock wave at the plane of maximum contraction, plane 3. As the value of P_6 is progressively reduced the shock becomes stronger and travels downstream towards plane 4. Ward-Smith (1979) continues:

"Due in part to viscous effects and, perhaps more importantly, the streamline curvature effects the compression shock will in practice differ from the plane discontinuity of one-dimensional flow theory. In particular, for $\delta < t/D < \varepsilon$, the region where the free shear layer reattaches to the wall of the orifice is, so far as the through-flow is concerned, effectively a concave corner, and once supersonic flow has been established between planes 3 and 4 it is from this locality that an oblique shock originates, giving rise to an oblique shock pattern downstream.

Whilst the shock stands in the region between the plane of maximum contraction, plane 3, and the reattachment plane 4, there exists the possibility of the shock modifying the geometry of the separation bubble. Only when a region of supersonic shock-free flow is established between planes 3 and 4 will the geometry of the separation bubble remain quite independent of the processes downstream and therefore it is only when this stage is reached that nozzles in the range $0 < t/D < \delta$ can finally be regarded as choked.

It is worth drawing special attention to a feature of the flow in nozzles satisfying the condition $\delta < t/D < \varepsilon$. Once supersonic conditions have been established downstream of the reattachment plane in these nozzles, the downstream conditions cannot influence the geometry of the separation bubble at the orifice entry. At the choked condition, therefore, all of these nozzles will have a separate flow pattern which is identical and is therefore entirely independent of t/D . This feature has a fundamental effect on the critical discharge coefficient of these nozzles, with important practical consequences."

In addition, as noted in Maestas (2015):

"A.J. Ward-Smith (1979), explored the critical discharge coefficient (C_d^*) for orifices. The critical discharge coefficient is the ratio of the actual discharge over the theoretical discharge of an orifice. Equations have been derived from governing laws and then used to calculate the theoretical discharge of an orifice based on perfect conditions and no losses. The discharge coefficient is used to

correct the calculated flow rate to match the actual flow rate. Ward-Smith presents a table of six combined references that list the critical discharge coefficient based on t/d , where t is the thickness of an orifice plate, and d is the diameter of the orifice. Ward-Smith also presents a graph of their own experimental results of a t/d range of 0.5 to 25, which shows that when t/d is between 1 and 7, the C_d value is constant. The 1/64-inch orifice plate (without an exit chamfer) that was used in this experiment, gives a t/d value of 8. This results in a slightly smaller C_d value as shown in Figure 2. For simplicity, it will be assumed that the C_d value for this orifice plate is the same as the others. Information from the Ward-Smith table relevant to this thesis research is summarized in Table 1 and the graph from Ward-Smith is found in Figure 2. It should also be noted that the data given in Ward-Smith may be considered in agreement with that of Perry (1949) if orifices having a $t/d \leq 0.14$ —since the data shown in Table 1 shows orifices with t/d ratios in this range did not choke. Further examination of these data may be fruitful.

Ward-Smith concludes the paper by stating:

The variations that exist (measurements fall in the band $0.81 < C_d^* < 0.86$) pinpoint two factors of crucial importance if this type of device is to be employed as a practical form of critical flowmeter. Firstly slight variation in the sharpness of the leading edge undoubtedly lead to variations in C_d^* . Secondly, because the orifice diameters of interest are so small, even slight inaccuracies in the measurement of the internal diameter of the nozzle can lead to significant discrepancies in the estimation of mass flow rate. This second factor is of course shared by all designs of critical flowmeter, and not just those with sharp upstream edges. There is little doubt that, with care, the effects of both of these factors can be reduced to small proportions.

Table 1. Critical Discharge Coefficients

References	t/d	Cd
Brain and Reid (1975)	0.28	0.841
	0.31	0.83
	0.488	0.844
	0.50	0.83
	0.51	0.83
	0.51	0.839
	0.54	0.845
	0.92	0.825
	0.986	0.835
	1.01	0.83
	1.01	0.83
	1.02	0.845
	1.933	0.82
	1.97	0.825
	2.00	0.841
	2.00	0.832
	2.07	0.843
	3.48	0.839
	4.92	0.826
Deckker and Chang (1965-66)	2	0.86
	1	0.86
	0.5	0.88
Jackson (1963)	0.33	0.845
	0.67	0.86
	1.0	0.835
	5.3	0.84
Grace and Lapple (1951)	1.00	0.83
Kastner, Williams, and Sowden (1964)	1.45	0.83
	1.473	0.832
	1.476	0.84
	1.433	0.832
	1.543	0.829
Rohde, Richards, and Metger (1969)	4.00	0.85
	2.83	0.86
	2.00	0.86

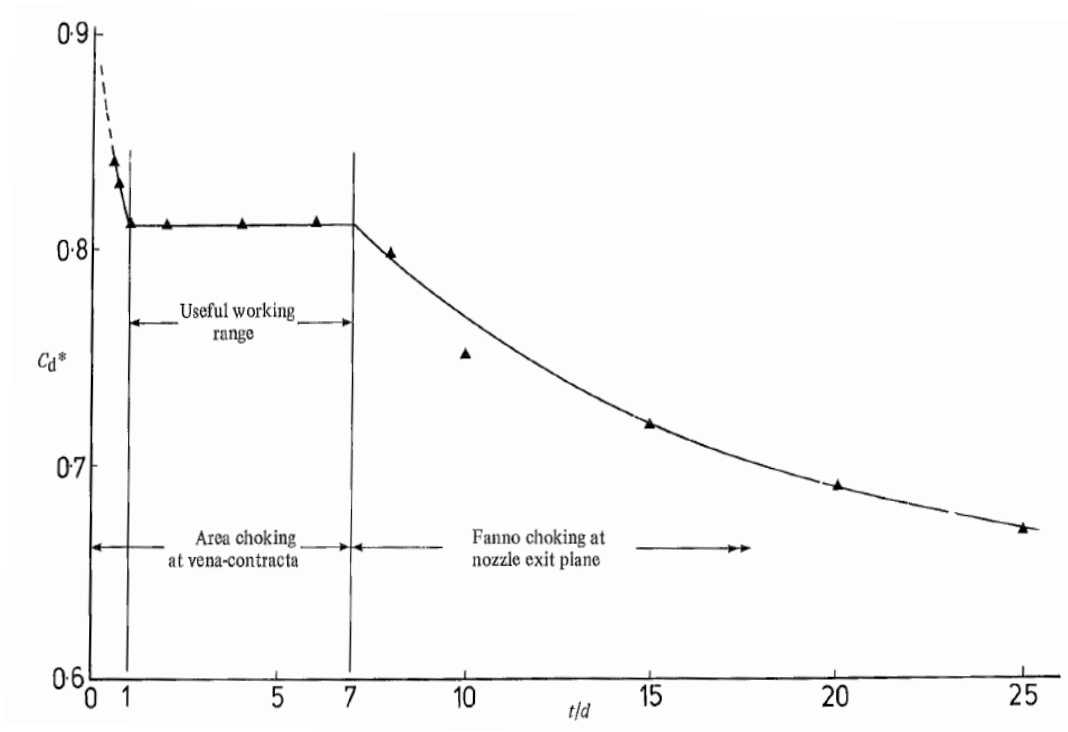


Figure 2. Graph showing the relationship between C_d and t/d . Ward-Smith (1979)

Ward-Smith states that variations in the discharge coefficient will exist due to the sharpness of the leading edge of the orifice and from inaccuracies in measuring the internal diameter of the orifice.”

Miller (1983) studied choking orifices, where he stated that choked flow is achieved by increasing the plate thickness. It was found that for a sharp edge and t/D ratios between 1 and 6, the discharge coefficient is 0.83932.

Miller (1983) also explored material about critical pressure ratios, where he stated that the downstream pressure P_d at which choked flow first occurs depended on the exit conditions. The critical pressure calculation is shown in Equation 1, where P_d is the downstream pressure, P_u is the total (stagnation) upstream pressure, and γ is the heat capacity ratio c_p/c_v of the gas.

Equation 1, critical pressure ratio.

$$\frac{P_d}{P_u} = \left(\frac{2}{\gamma + 1} \right)^{\frac{\gamma}{\gamma - 1}}$$

Uncertainty on orifice flow measurement is an important factor to consider when predicting gas critical flow using orifice plates. Husain (1995) states that major factors contributing to the flow meter uncertainty for a thin, concentric, square edge flow meter are “the predictability of flow profile, fluid properties at flowing condition, precision of empirical equation for discharge coefficient, manufacturing tolerances in meter components, and the uncertainty associated with secondary devices monitoring the static line pressure, differential pressure across the orifice plate, flowing temperature, etc. An orifice flowmeter is a very forgiving device and for most applications, with normal care in installation and instrumentation, the measurement accuracy is consistently better than ± 1 %. If the measurement error is greater than ± 1 %”.

Husain (1995) concludes that errors stem from uncertainties in the quantities used on the flow equation, actual physical properties of the flowing fluid, and dimensions of the flow meter. Therefore, fluid properties should be supervised to achieve the best achievable accuracy.

Lastly, there are finite pressure disturbances which may be present when recording critical gas measurements. This pressure disturbances have a thickness that are on the order of free molecular paths and consequently they appear as discontinuities in the flow and are called shock waves. These shock waves contribute to the uncertainty or inefficiency of orifice meters. Dosanjh (1956) studied the wave pattern occasioned from impact of an incident shock wave with a grid-like obstacle. With the help of a shadowgraph photography, he examined the wave patterns developed far upstream and far downstream of the orifice. Dosanjh was the first to

observe and explain the choking phenomenon observed in the supersonic flows immediately downstream of the grid-like obstacle. Franks (1957) utilized a rotating drum camera schlieren system and a Mach Zehnder interferometer for taping the wave pattern and the immediate density scatterings in the various regions resulting from the shock wave–grid contact. Franks also detected the manifestation of a choking shock wave at the grid exit and proposed the analytical solution to this flow.

Barthel (1957) showed that the shock wave–orifice interaction might stem in either of three different flow patterns. The first pattern, which occurs when the incident shock wave is weak, results in an un-choked flow through the orifice. The second pattern for stronger shocks, emerges in sonic velocity at the orifice throat. The third wave pattern for stronger incident shock waves, the auxiliary shock at the exit of the orifice’s flow becomes a traveling shock; its strength decreases until finally it becomes a rarefaction wave.

Zucker & Biblarz (2002) concluded that if conditions of the shock are known ahead of time, a specific set of circumstances must exist after the shock. Clear results can be found for the lastly, a shock wave is a type of compression process, though a rather ineffective one since fairly large losses are found in the process. In flow measurement on orifice one must account for such losses.

Summary of literature review:

1. Critical flow can be achieved in orifices with t/D ratios ranging between δ and ϵ , where the choked flow will not vary as the critical pressure ratio decreases.
2. The range of δ and ϵ , where true critical flow occurs, depends on roughness. For sharp edge orifices, δ varies from ~ 0.3 to ~ 1 . For rough bores $\epsilon \sim 7$, and for smoother bores ϵ can be as much as ~ 10 .
3. The expression on Equation 1 is applied to obtain the critical pressure ratio for a choked orifice within a t/D range.
4. For orifices with an appropriate t/D range for critical flow, the shock wave is located within the orifice itself since only orifices considered as cylindrical nozzles with sharp upstream edges can be used to measure critical flow accurately.
5. The discharge coefficient is used to correct the calculated flow rate to match the actual flow rate. C_d has a constant value of 0.839 for $1 < t/D < 6$.
6. Errors in critical gas flow measurement are due to uncertainties of the quantities used in flow equation, actual physical properties of the flowing fluid, and dimensions of the flow meter. Therefore, fluid properties should be supervised with best achievable accuracy.

Section III: Description of Hardware and Instrumentation

The hardware and instrumentation specifics for the experimental apparatus (Figures 3, 4, 5. Table 2 and 3) were obtained from Maestas (2015).

Hardware

This section describes the hardware used to assembly the experiment apparatus, which was built to test the critical orifice plate. Table 2 specify the hardware's characteristics such as its model, manufacturer, range, and measurement uncertainties. Figure 3 gives a visual representation of the apparatus's hardware with the purpose of describing the specified components in Table 2.

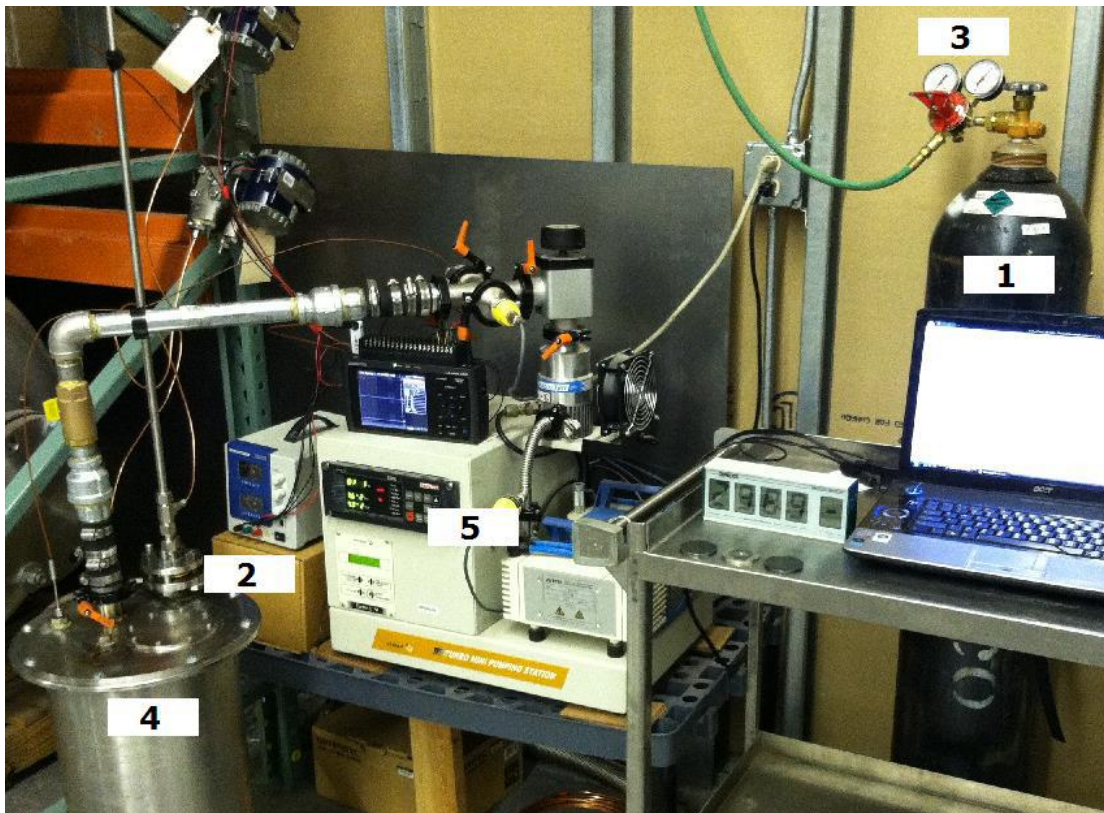


Figure 3. Experimental apparatus used in Maestas (2015).

Table 2. Major components of experimental apparatus used in Maestas (2015).

List	Name	Model Number	Range	Manufacturer
1	Nitrogen tank	Not available	Not available	Norco
2	Orifice plate	Not available	Not available	Not available
3	Pressure regulator	30-100-540	0-3000 psi	Smith
4	Receiver vessel	Not available	Not available	Not available
5	Vacuum pump	Turbo-V-70	1E-09 Torr	Varain

For the experiment test, the nitrogen cylinder provides the working fluid that flows at fixed pressure, maintained by a regulator, through the entrance line until it reaches the orifice plate, and then down to the receiving vessel.

The flowing fluid is 99.99% pure commercial grade nitrogen gas. The source of nitrogen was provided by a Norco (company's name) nitrogen bottle. The regulator was required to maintain a fixed pressure just upstream of the orifice at a constant 19~20 psig. The pressure regulator was a Smith model number 30-100-540, which had a 3000 psig maximum inlet pressure, a 0-100 psig range supply pressure, and a +/- 2% actual gauge reading for the pressure regulator and flow gauges.

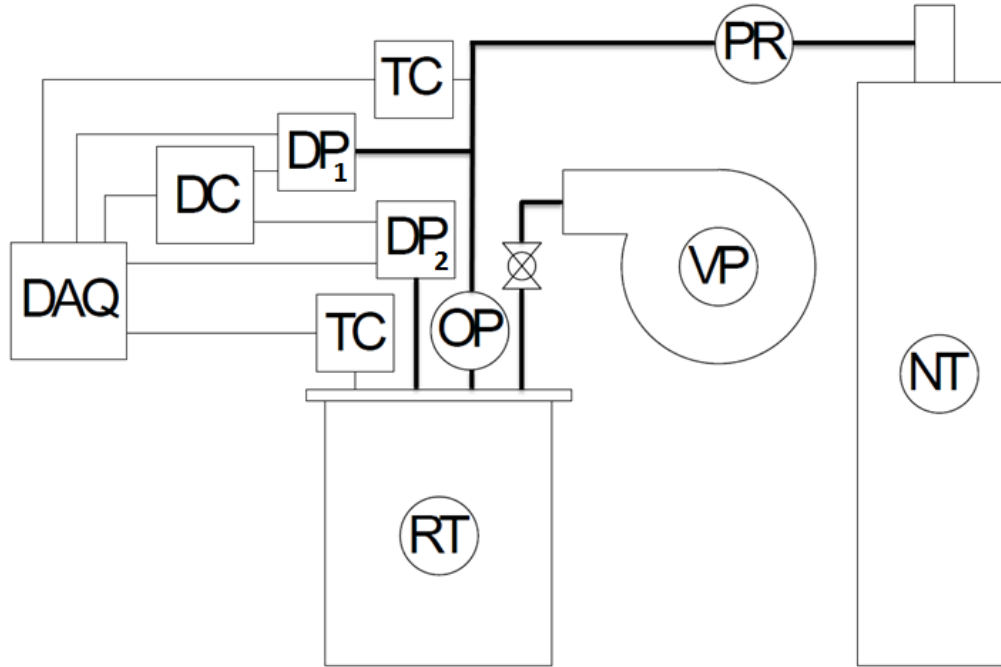
The nitrogen flowing through the orifice plate was collected in the receiver vessel. The receiver vessel was designed to operate at a perfect vacuum with negligible distortion. The tank was constructed of a quarter inch thick stainless steel with a groove for an O-ring to seal the lid to the body. A vacuum pump was utilized to evacuate the receiving vessel prior to each experiment. A valve was used to connect the tank and vacuum pump. During testing, the valve was closed to limit the control volume to that downstream of the valve. The vacuum pump is a Varian Turbo-V-70 with k-type vacuum fittings, which include a tightening collar and a rubber O-ring gasket. Per the vacuum pump's manufacturer specifications, pressures as low as 1×10^{-9}

Torr are possible. The test procedure described in Maestas (2015) reduced the receiver vessel pressure to near zero prior to each experiment.

Finally, three orifice plates were constructed for the experiment with throat diameters of 1/16-inch, 1/32-inch, and 1/64-inch diameter. An additional orifice plate with a 1/64-inch throat diameter and a chamfered leading edge throat geometry was available from earlier experiments and was also included in the experiments [Maestas (2015)]. The plates were constructed of 1/8-inch thick cold rolled, low carbon steel. The ratios of the orifice throat diameter (d) to the upstream line diameter (D) were: 1/16-inch \rightarrow 0.1453, 1/32-inch \rightarrow 0.07267, and 1/64-inch \rightarrow 0.0372. The orifice plate thickness (t) to the orifice throat diameter (d) ratios were: 1/16-inch \rightarrow 2, 1/32-inch \rightarrow 4, 1/64-inch \rightarrow 8, and 1/64-inch chamfered leading edge geometry \rightarrow 2.

Instrumentation

Figure 4 shows the experiment piping and instrumentation diagram.



	Instrument
	Hardware
	Valve
	Nitrogen Line
	Instrument Electrical
DAQ	Data Acquisition System
DP ₁	Differential Pressure Transducer (25 psid)
DP ₂	Differential Pressure Transducer (300 inch)
TC	Thermocouple
DC	DC Power Supply
NT	Nitrogen Tank
OP	Orifice Plate
PR	Pressure Regulator
RT	Receiver Tank
VP	Vacuum Pump

Figure 4. Experiment Hardware and Instrumentation.

For the experiment apparatus, Table 3 describes the instrument's name, model number, manufacture, range and uncertainty. Figure 5 demonstrates the arrangement of the instrumentation while listing the specified characteristics in the Table 3.

Table 3. Instrumentation identification.

	Name	Manufacturer	Model Number	Range	Uncertainty	
1	Barometer	Conex Electro-Systems	Model JDB-1	9.8-15.2 psia	+/-	0.025 psi
2	Data Acquisition System	Graphtec Corp.	Midi Logger GL820	0-50 volts	+/-	0.05 volts
3	300 inch H2O Differential Pressure Transducer	Omega Engineering	PX771A-025DI	0-10.84 psi	+/-	0.01626 psi
4	25 psid Differential Pressure Transducer	Omega Engineering	PX771A-300WCDI	0-25 psi	+/-	0.0375 psi
5	K Type Thermocouples	Idaho Laboratories Corp.	K-Type	0-150°F	+/-	1°F
6	Power Supply	BK Precision	1710A 30B/1A	0-30 Volts	+/-	NA
NA	Pressure Calibrator	Beta	Beta Gauge PI PRO	NA	+/-	0.05% FS

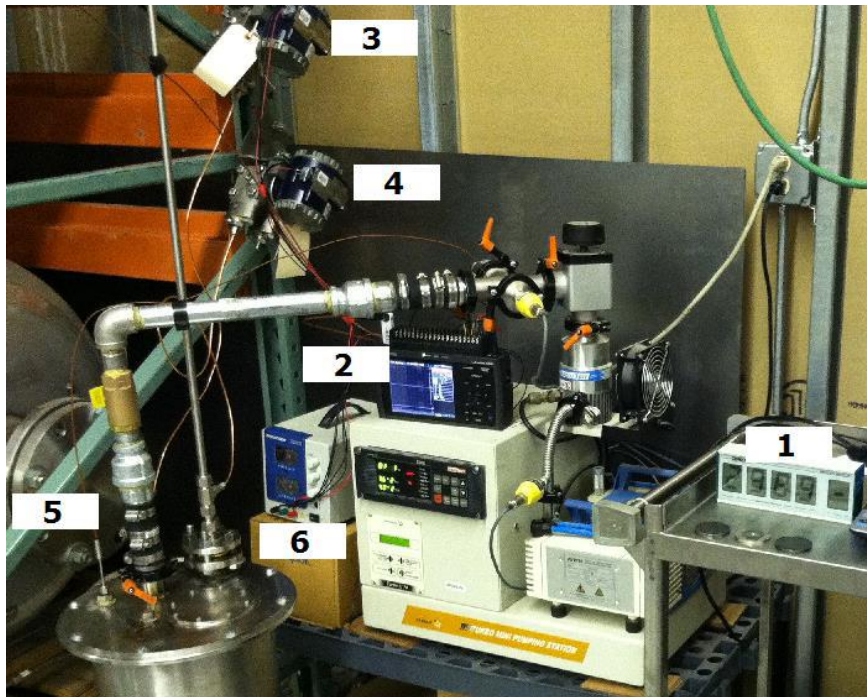


Figure 5. Instrumentation arrangement.

A more detailed information for the both the hardware and measuring instrumentation for the experiment, can be found on Maestas (2015).

Section IV: Hand calculations

This section describes the approach to hand calculation to check COMSOL calculations.

Table 4 describes the critical mass flow rates from Maestas (2015) which were calculated using Equation 2 from Miller (1983). Equation 2 is used to check COMSOL calculations.

Table 4. Hand calculation critical mass flow rate.

Orifice diameter (in)	t/D	Theoretical Standard mass flow rate (kg/s)
1/16	2	8.4027E-4 +/- 1.239E-5
1/32	4	2.0928E-4 +/- 4.359E-6
1/64	8	5.4305E-5 +/- 1.562E-6
1/64 inch Chamfered	8	5.7455E-5 +/- 1.651E-6

Equation 2, Standard Critical Mass Flow Rate with Discharge Coefficient.

$$\dot{m} = C_d A \sqrt{\gamma \rho P_t \left(\frac{2}{\gamma + 1} \right)^{\frac{\gamma+1}{\gamma-1}}}$$

P_t is the total upstream pressure, A is the cross-sectional area of the orifice, γ is the heat capacity ratio, ρ is the upstream stagnation density, and C_d is the discharge coefficient. Brian & Reid (1975) indicates that the coefficient of discharge for a sharp edge orifice C_d is 0.839 *if* it meets the following condition:

$$1 < t/d < 10$$

Where t is the thickness of the orifice plate, and d is the diameter of the orifice.

Section V: COMSOL

This section describes COMSOL software, and the elements used to build the CFD model of the gas flow through the orifice plate and downstream receiver vessel. The COMSOL elements include: space dimension, geometry, material, fluid flow interface, turbulence model, meshing, study, and post-processing analysis.

COMSOL software description and computing specifications

COMSOL Multiphysics is a cross-platform finite element analysis, solver and Multiphysics simulation software package. It allows conventional physics-based user interfaces and coupled systems of partial differential equations (PDEs). COMSOL provides an interdigitated electrode (IDE) and unified workflow for fluid applications.

The software provides a powerful integrated desktop environment with a *Model Builder* that gives you a full overview of the model and access to all functionality (see Figure 6). COMSOL Multiphysics can easily extend conventional models for one type of physics into Multiphysics models that solve coupled physics phenomena — and that do so simultaneously. Accessing this power does not require an in-depth knowledge of mathematics or numerical analysis.

Using the built-in *physics interfaces* and the advanced support for material properties, you can build models by defining the relevant physical quantities — such as material properties, loads, constraints, sources, and fluxes — rather than by defining the underlying equations. COMSOL can always apply these variables, expressions, or numbers directly to solid and fluid domains, boundaries, edges, and points independently of the computational mesh. The COMSOL Multiphysics software then internally compiles a set of equations representing the entire model.

COMSOL Multiphysics can be accessed as a standalone product through a flexible graphical user interface.

(GUI), in applications created using the Application Builder, or by script programming in Java® or the MATLAB® language (this requires a LiveLink™ *for* MATLAB® license).

Using these physics interfaces, COMSOL can perform various types of studies including:

- Stationary and time-dependent (transient) studies
- Linear and nonlinear studies
- Eigen-frequency, modal, and frequency response studies

When solving the models, the COMSOL Multiphysics software assembles and solves the problem using a set of advanced numerical analysis tools. The software runs the analysis together with adaptive meshing (if selected) and error control using a variety of numerical solvers. The studies can make use of multiprocessor systems and cluster computing, and you can run batch jobs and parametric sweeps. The COMSOL Multiphysics software creates *sequences* to record all steps that create the geometry, mesh, studies and solver settings, and visualization and results presentation. This makes it easy to parameterize any part of the model; simply change a node in the model tree and rerun the sequences. The program remembers and reapplies all other information and data in the model.

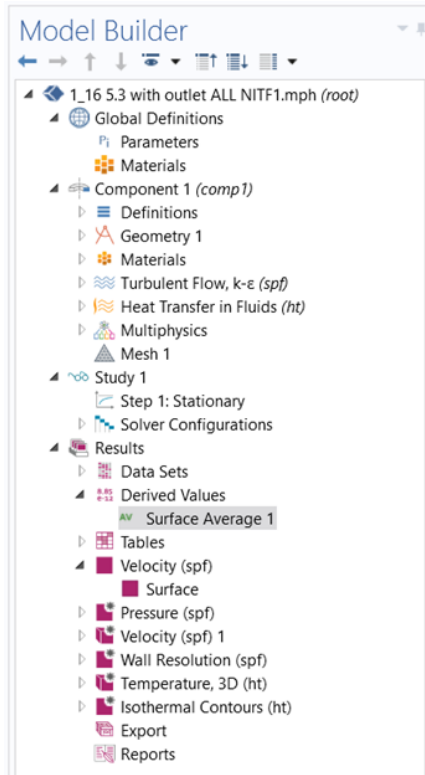


Figure 6. COMSOL model builder tree.

Table 5 describes the COMSOL software version, manufacturer, as well as the computer's model, RAM, and frequency.

Table 5. Computer and COMSOL specifications.

Operator	Windows 10
Processor	Intel® Core™ i7-6700HQ CPU @ 2.60GHz
Installed memory (RAM)	16.0 GB
System Type	64-bit Operating System, x64-based processor
Computer name	DESKTOP-N5J0NJ9
Computer model	P57F
Computer Manufacturer	Dell
COMSOL Version	5.2
COMSOL License number	4077083
COMSOL Modules	<ul style="list-style-type: none"> • Non Isothermal Turbulent Flow • High Mach Number Flow
COMSOL Manufacturer	COMSOL Group

Space dimension

Figure 7 describes the space dimensions that COMSOL offers to the user. A two-dimensional (2-D) model is used for these studies. If the calculations had converged, a three-dimensional model would have been constructed—but unfortunately calculational convergence was never achieved even for the 2-D model.

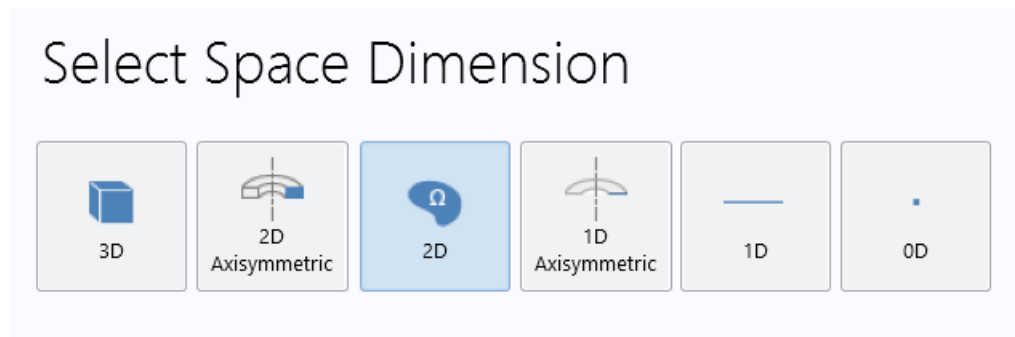


Figure 7. COMSOL space dimension.

Geometry

The geometric features include 4 rectangles connected by a union Boolean operation. In COMSOL, rectangles on 2-dimensional model represent cylindrical pipes. Figure 8 shows the front view of the device model.

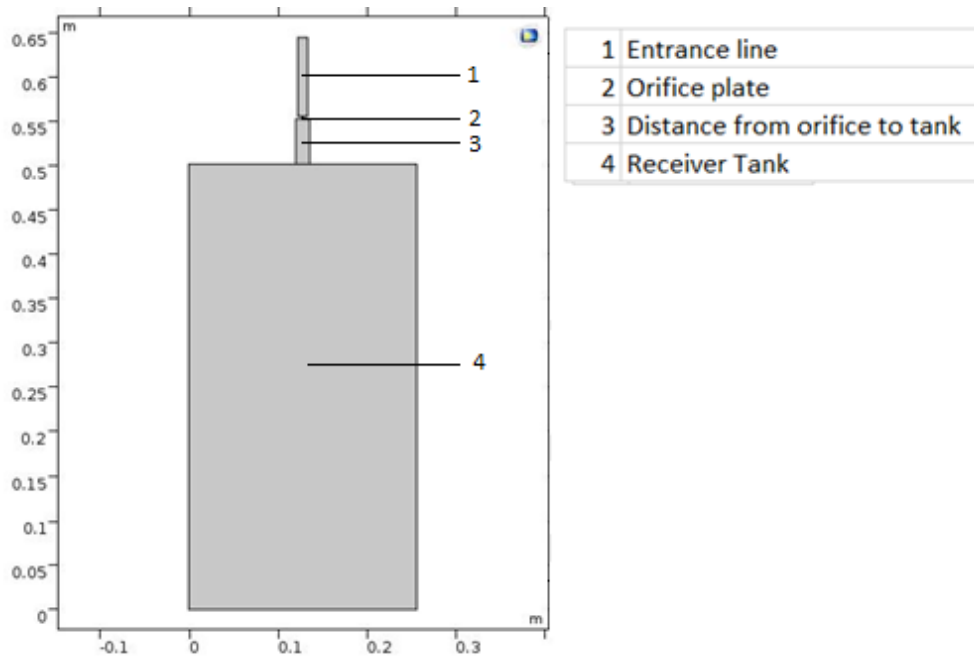


Figure 8. 2D geometry model.

Material

From the material library, nitrogen gas is added to model as the working fluid. The material properties include density, dynamic viscosity, thermal conductivity, heat capacity, ratio of specific heats, and the gas constant. Figure 9 illustrate material properties.

Material Properties					
Material Contents					
»	Property	Name	Value	Unit	Property group
<input checked="" type="checkbox"/>	Heat capacity at constant pres...	Cp	1040	J/(kg·K)	Ideal gas
<input checked="" type="checkbox"/>	Ratio of specific heats	gamma	1.4	1	Ideal gas
	Mean molar mass	Mn	28	kg/mol	Ideal gas
<input checked="" type="checkbox"/>	Thermal conductivity	k	k_gas_4(...	W/(m·K)	Basic
	Heat capacity at constant pres...	Cp	C_gas_3(...	J/(kg·K)	Basic
<input checked="" type="checkbox"/>	Density	rho	rho_gas(...	kg/m ³	Basic
<input checked="" type="checkbox"/>	Dynamic viscosity	mu	eta(T[1/...]	Pa·s	Basic
	Ratio of specific heats	gamma	1.4	1	Basic
	HC	HC	HC_gas(...	J/(mol·K)	Basic
	Specific gas constant	Rs	296	J/(kg·K)	Ideal gas

Figure 9. Material contents.

Fluid flow interface

The nitrogen gas flowing through the orifice plate into the receiving tank will reach sonic velocities, and experience temperature and density changes, therefore the fluid flow is identified as High Mach number (Mach number greater than 0.3) non-isothermal compressible flow. Figure 10 below identifies the only COMSOL fluid flow interface which applies to this problem: High Mach Number Flow turbulent flow (hmnf).

The next step is to choose the right turbulence model.

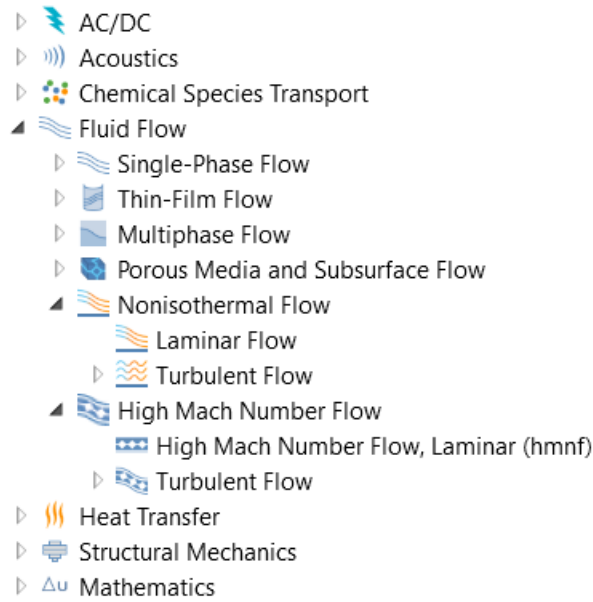


Figure 10. COMSOL physics modules.

Turbulence model

The discharged nitrogen gas into the receiving vessel is a jet flow, therefore the turbulence model must be able to accurately compute jet flows. Frei (2017) states $k-\omega$ model is useful in internal flows, flows that exhibit strong curvature, separated flows, and jets. Therefore, $k-\omega$ is selected as the turbulence model for this study.

However, hmnf interface doesn't include a $k-\omega$ model. It only contains $k-\epsilon$ and Spalart-Allmaras models, neither of which can very accurately compute flow fields that exhibit adverse pressure gradients, strong curvature to the flow, or jet flow. However, given that this is the only capability available in COMSOL the calculation is performed using the k -epsilon turbulence model to provide a baseline for further study once an appropriate turbulence model is included in the COMSOL Multiphysics package in the future.

Meshing

The Mesh features enable the discretization of the geometry model into small units of simple shapes, referred to as mesh elements. For a 2-D model, the mesh generator discretizes the domains into triangular or quadrilateral mesh elements. If the boundary is curved, these elements represent only an approximation of the original geometry. The sides of the triangles and quadrilaterals are called mesh edges, and their corners are mesh vertices. The boundaries defined in the geometry are discretized (approximately) into mesh edges, referred to as boundary elements (or edge elements), which must conform to the mesh elements of the adjacent domains. The geometry vertices are represented by vertex elements.

Moreover, COMSOL includes a physics-controlled meshing in which nine predefined mesh size settings ranging from "Extremely fine" to "Extremely coarse" are available. Figure 11 demonstrates the nine mesh size settings and coarse mesh statistics. The finer the mesh the longer it takes to compute the study, but a more accurate result can be expected.

Additionally, COMSOL counts with an adaptive mesh refinement, where an error estimation strategy is employed to determine the point in the modeling domain where the local error is largest. An acceptable mesh error should be at least smaller than 10^{-6} because COMSOL error plots for a finite element solution showed that the error would decrease as low as 1.5×10^{-8} before it starts to go back up. Frei (2013) states that in order to be on the safe and practical side a minimal achievable error is 10^{-6} . The Finite Element Method (FEM) software then takes this error estimation and applies the data to create an entirely new mesh. Smaller elements are used in regions where the local error is significant, and the local error throughout the model is considered. The benefit here is that COMSOL will do all of the mesh refinement.

For this COMSOL study, a coarse mesh was selected. Figure 12 shows the coarse meshing on the geometry.

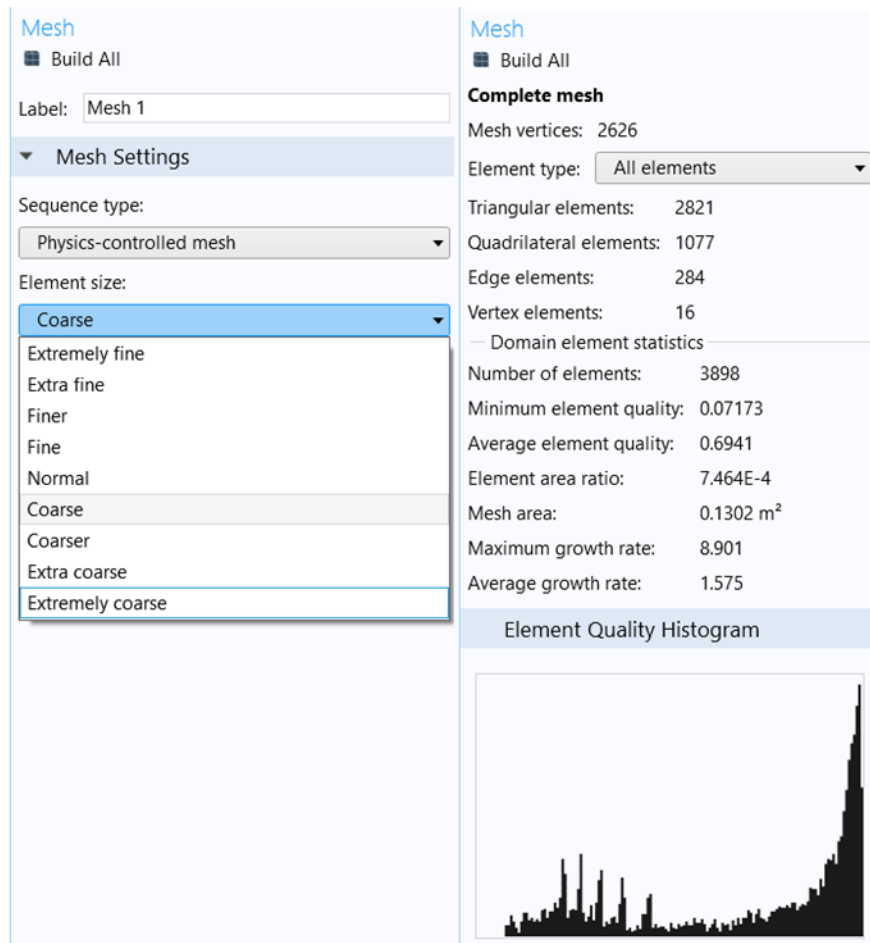


Figure 11. Predefined mesh size settings and statistics.

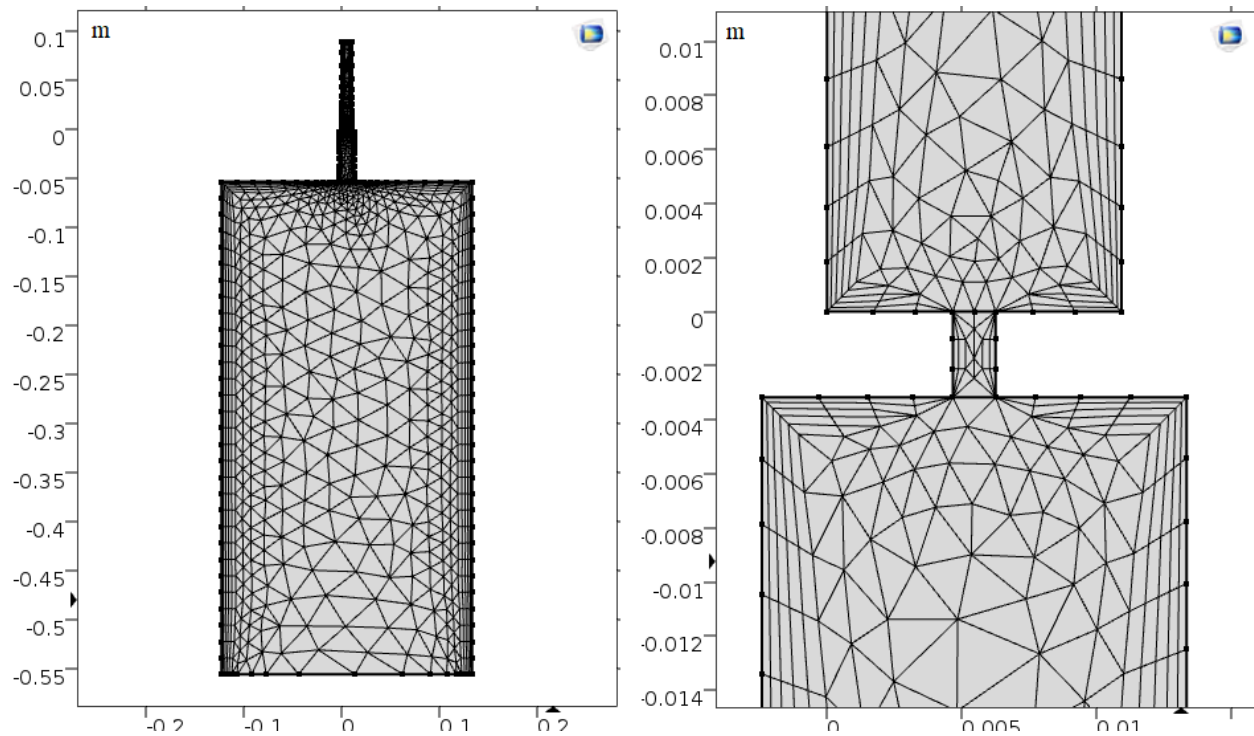


Figure 12. Coarse meshing. Full system meshing (left). Orifice meshing (right).

Study

Once the meshing is done, the next step is to determine which study is the most suitable to use in order to get an accurate flow simulation. The study node for this COMSOL version includes different types of studies such as Stationary, time-dependent, and Thermal perturbation, Frequency Domain. For this analysis, a time-dependent study is the first option to choose because it is desired to know how the flow behavior on the entire system varies with time and how it affects the velocity and pressure profiles. After all, the experimental method was conducted for a period of time as well. However, before choosing a time-dependent study, it is important to identify whether the gas in the receiving vessel is rarefied or continuum. The rarefied condition is only possible in the receiver tank since the tank is initially at vacuum conditions at the beginning of the experiment. However, the rarefied condition is not always

present in the experiment because the pressure inside the tank will eventually increase, and then at some point the gas becomes a continuum in the receiver tank.

Rarefied gas flow:

A rarefied gas flow is described as the fluid dynamics of gas in which the mean free path of the molecules is larger than the size of the vessel they are. For small sized tubes, this means pressures well below 1.45E-5 psia. This is also called the regime of high vacuum.

The principal parameter of rarefied gas dynamics is the Knudsen number (Kn). Knudsen number is the ratio of molecular mean free path length λ to a physical length scale L (the physical length can be the tube length or the orifice diameter for this case). Equations 3 and 4 define the Knudsen number [Sharipov (1998)].

Equation 3, Knudsen Number.

$$Kn = \frac{\lambda}{L}$$

Equation 4, Knudsen Number alternative.

$$Kn = \frac{\mu}{\rho D} \sqrt{\frac{\pi m}{2K_B T}}$$

Where μ is the dynamic viscosity, ρ is the gas density, m is the molecular mass, T is the thermodynamic temperature, D is the orifice diameter, and K_B is the Boltzmann constant. If $Kn < 0.01$, then the gas flow is continuum. If $Kn > 0.01$, then the gas flow is rarefied. Detailed calculation of Knudsen number is found in Appendix A.

Calculation of The Knudsen equation showed the there is a rarefied gas flow inside the receiver tank at the beginning of the experiment. A rarefied gas flow simulation on COMSOL will require the use of a special module called “Free Molecular module”. Unfortunately, this module was not available on the COMSOL 5.2 version used for this simulation. As a consequence, a time-dependent study without an outlet boundary is not feasible.

However, COMSOL should be able to calculate this problem as a time-dependent problem if there is enough nitrogen present in the receiver tank that the gas is no longer rarefied in the tank, then calculations can be performed between the time when the Knudsen number indicates a continuum exists in the tank and when the pressure ratio is less than the critical pressure ratio. For this COMSOL calculation, a stationary study with a critical pressure ratio is selected to compute. The critical pressure ratio can be calculated using Equation 2 from Miller (1983).

Post Processing Analysis

In the post processing and visualization, a combination of arrow and surface plots were used to see the velocity and pressure profiles on the entire model. On the results node, an average surface derivation option is selected to calculate the average velocity, and density at the orifice surface. Both of these values are plugged into Equation 5 to calculate the critical mass flow rate, where V is the average velocity of gas at the orifice, ρ is the average density at the orifice, and A is the cross-sectional area of the orifice. Figure 13 shows the steps to calculate the average surface velocity and density.

Equation 5, Mass flow rate.

$$\dot{m} = \rho V A$$

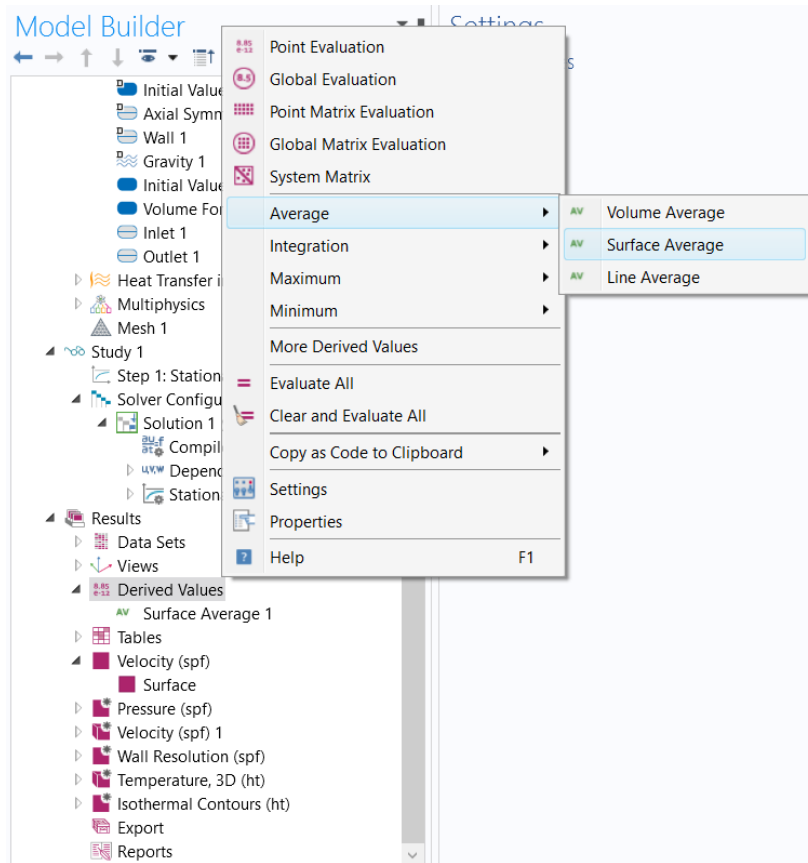


Figure 13. Post processing analysis steps.

Section VI: COMSOL calculations

A total of 3 calculations were performed for each orifices. The hmnf k-ε studies were run with the boundary conditions described Table 6 and 7. Then COMSOL calculated flow rates are compared to rates from Equation 2 [Miller (1983)] using Equation 6 below. The COMSOL calculation procedure can be found on Appendix B.

Table 6. Inlet and Outlet pressure cases.

Case #	Orifice diameter	t/D	Receiving tank?	Inlet pressure (psia)	Outlet pressure (psia)
1	1/16-inch	2	YES	31.24	16.48
2	1/32-inch	4		31.24	16.48
3	1/64-inch	8		31.24	16.48

Table 7. Boundary conditions.

Ambient temperature	292.7 K
Ambient pressure	12.5 psi
Inlet temperature	292.7 K
Outlet temperature	291.4 K
Material	Nitrogen gas
Y	1.4
Rgas	296 J/kg/K

Equation 6, Percent change Formula.

$$\%Change = \left(\frac{\dot{m}_{\text{standard}} - \dot{m}_{\text{COMSOL}}}{\dot{m}_{\text{COMSOL}}} \right) * 100$$

Section VII: Results

High Mach number Flow k- ϵ

Table 8 shows that COMSOL flow rates compare well with the standard equation flow rate for the last two t/D ratios, however for ratio of 2, the COMSOL mass flow rate doesn't compare as well. Therefore, the hmnf k- ϵ calculated flow rates don't agree with Ward-Smith (1979), where it is stated that for t/D ratios between 2 and 8, the correct mass flow rates can be calculated by using a constant critical pressure ratio.

After doing some trial and error calculations for the t/D of 2 case, COMSOL was able to obtain a good comparable flow rate by increasing the critical pressure ratio or increasing the downstream pressure to 18.3 psia. The result was 8.3942E-4 kg/s, which is a percent change of 0.1% with respect to the standard equation described in Miller (1983).

Table 8. Hmnf k- ϵ mass flow rates.

Orifice diameter (in)	t/D	COMSOL mass flow rate (kg/s)	Standard mass flow rate (kg/s)	Comparison
1/16	2	7.4016E-4	8.4027E-04	-13.5%
1/32	4	2.1523E-4	2.0928E-04	+2.76%
1/64	8	5.7003E-5	5.4305E-05	+4.73%

Figures 14-16 show that the nitrogen gas velocity rapidly increases when it reaches the orifice, and then the velocity decreases when it reaches the downstream region. However it is observed that the jet flow is not symmetrically distributed once the flow passes through the orifice.

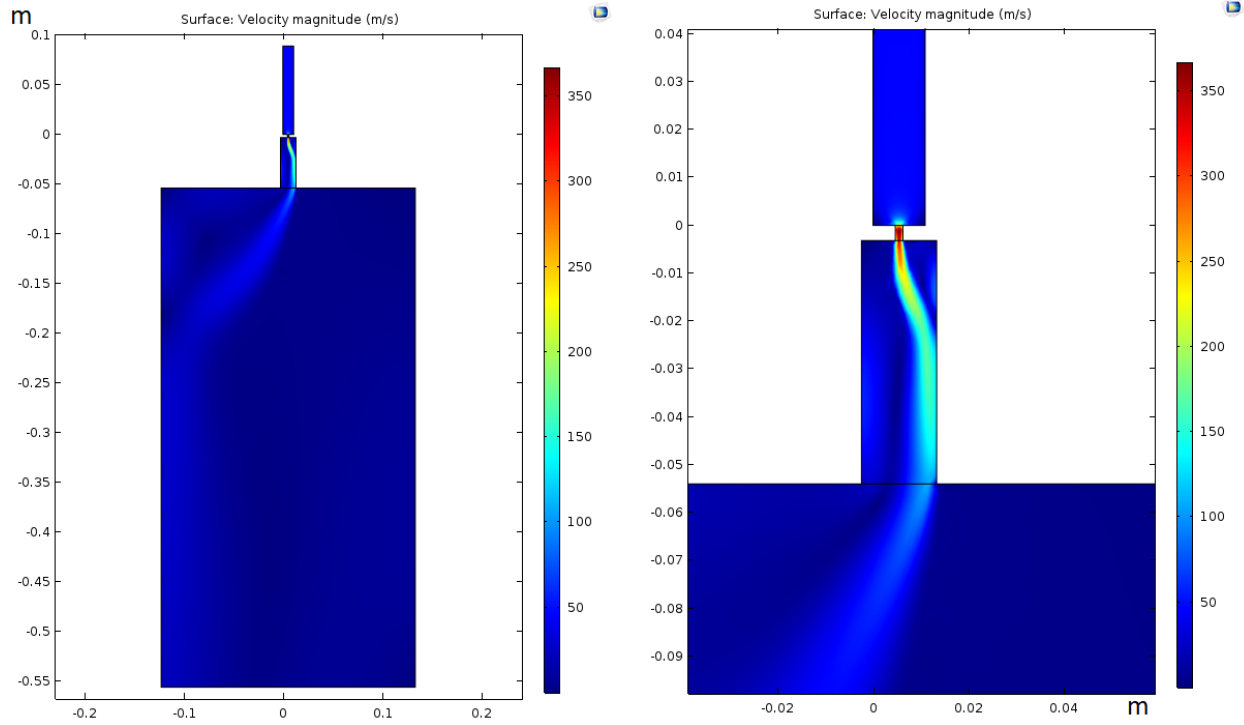


Figure 14. Hmnf k- ϵ , velocity profile, 1/16 inch.

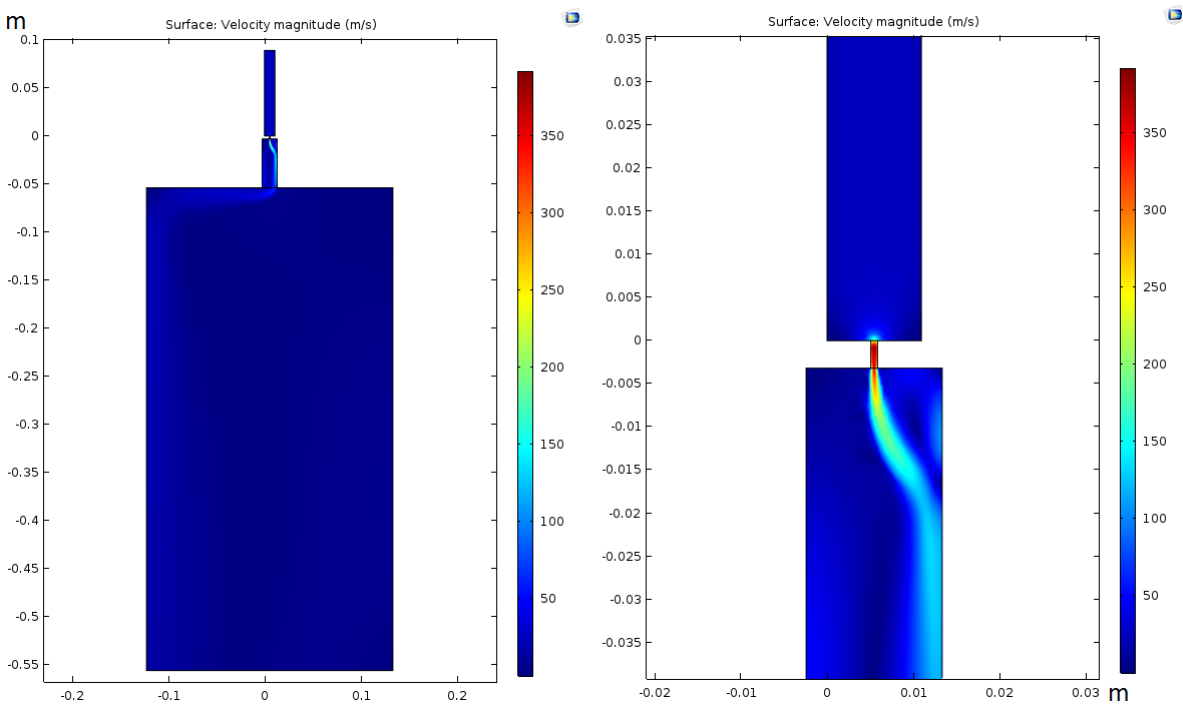


Figure 15. Hmnf k- ϵ , velocity profile, 1/32 inch.

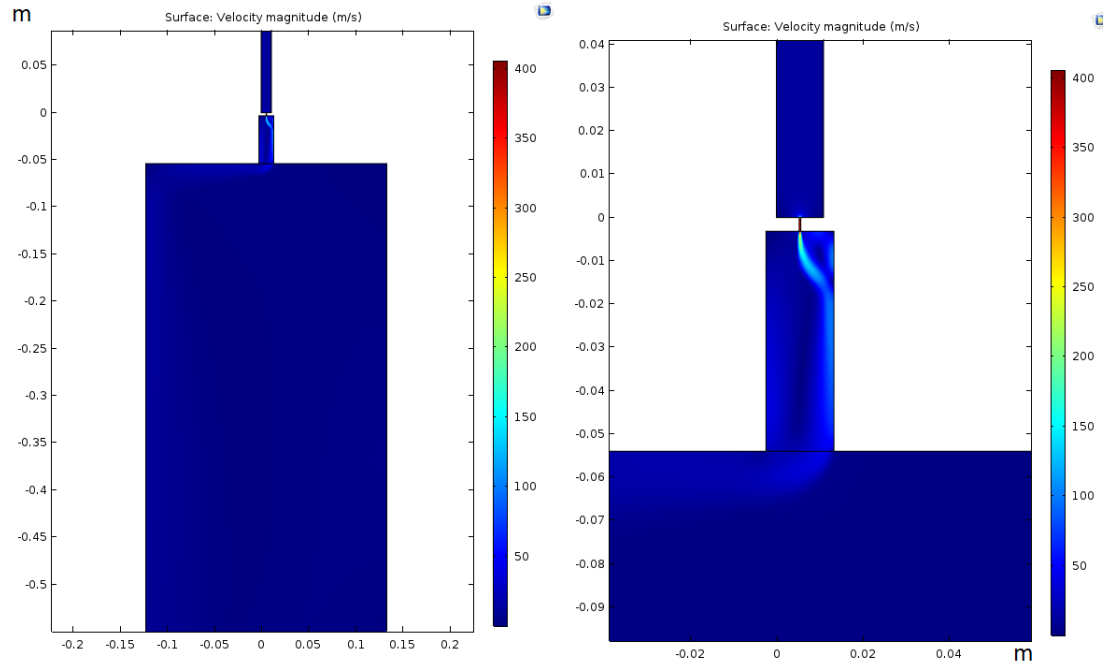


Figure 16. Hmnf k- ϵ , velocity profile, 1/64 inch.

Figures 17-19 show how the pressure suddenly drops at the orifice entrance. This type of behavior is expected to happen since the fluid becomes choked at the orifice. A choked flow prevents the downstream from interacting to the upstream pressure.

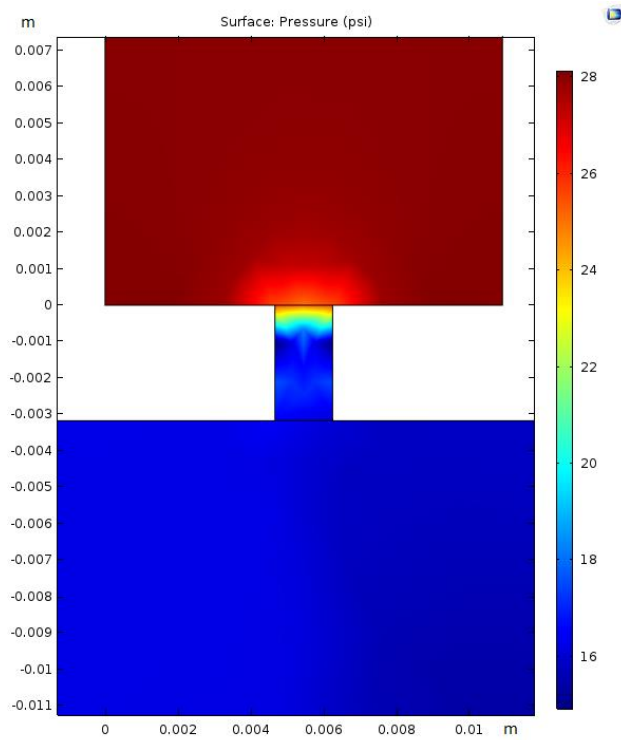


Figure 17. Pressure profiles at the orifice: 1/16 inch (hmnf k- ϵ).

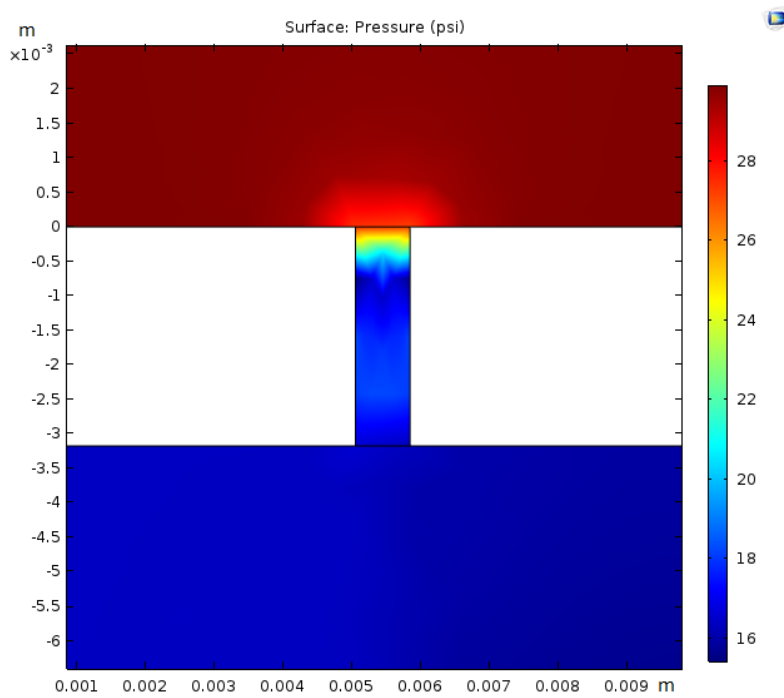


Figure 18. Pressure profiles at the orifice: 1/32 inch (hmnf k- ϵ).

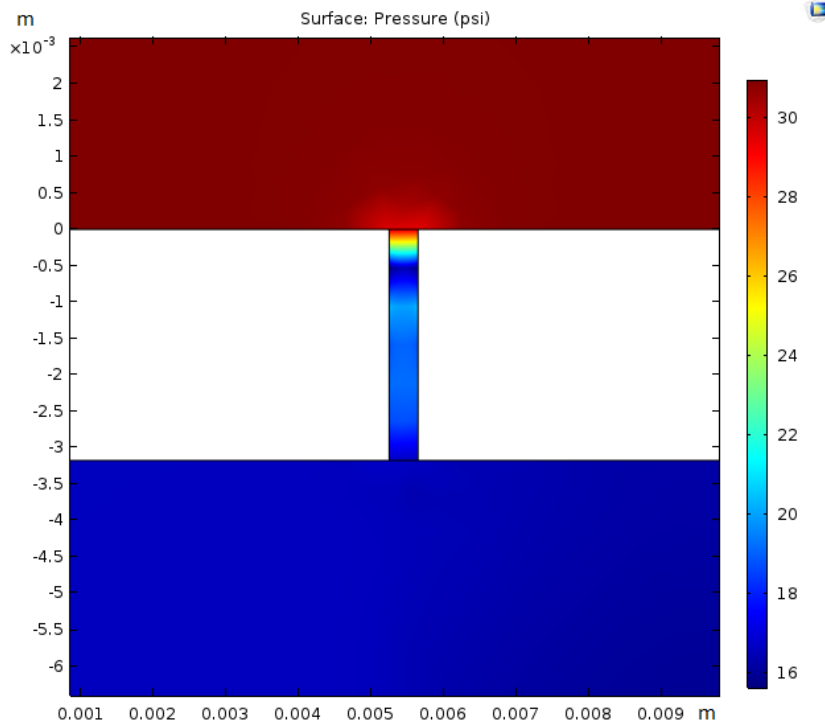


Figure 19. Pressure profiles at the orifice: 1/64 inch (hmnf k- ϵ).

COMSOL wasn't able to calculate the correct mass flow rate for t/D ratios ranging between 2 and 8 for a constant critical pressure ratio as stated by Ward-Smith (1979). Lastly, COMSOL wasn't able to accurately predict the thermodynamic state in the downstream receiving vessel because the jet flow coming from the orifice was not symmetrically distributed through the vessel.

Grid Convergence study

Approximation to the real solution is relied on. The aim of the Mesh refinement study or grid convergence study is to show that the solution converges. Convergence is achieved when the calculations give the same solution within an acceptable uncertainty band. An acceptable convergence uncertainty should be at least smaller than 10^{-3} .

All three cases were calculated using a discretization of second order accuracy. This study determined whether or not the answer diverges or converges as the mesh size decreases. Three different meshes were computed; coarse, normal, and fine. For the hmnf k- ϵ , Figure 20 compares the convergence plot for the 1/64-inch case, and Table 9 compares the mass flow rate solution between meshes.

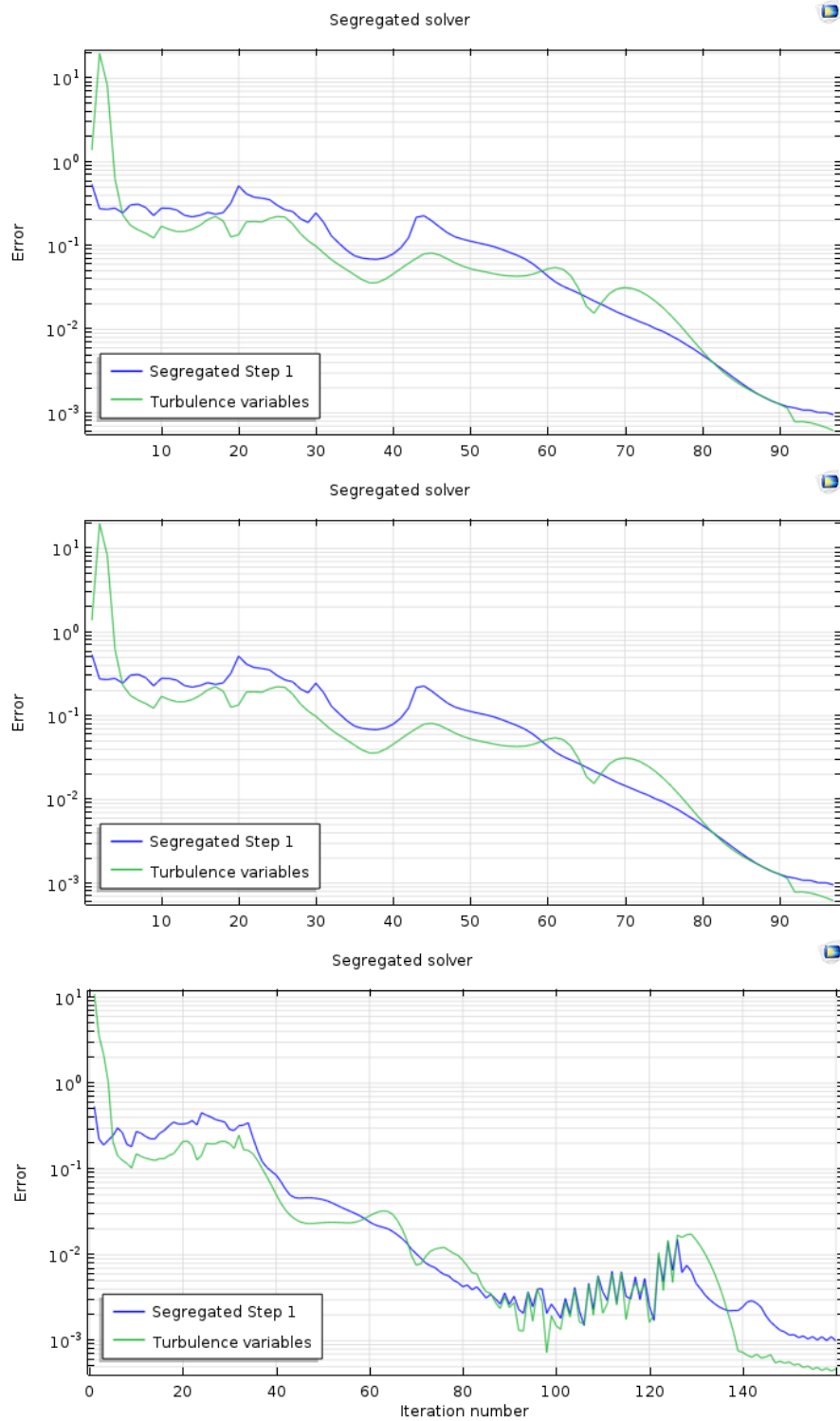


Figure 20. Convergence plot, hmnf k- ϵ . Coarse (higher), normal (middle), fine (lower).

Table 9. Mesh size solution (1/32", hmnf k- ϵ).

Mesh	Mass flow rate (kg/s)
Coarse	2.1523 E-4
Normal	2.1463 E-4
Fine	2.2215 E-4

Figure 20 shows that for increasing numbers of time steps, the various important residuals decrease until they're below a defined threshold, and it shows that COMSOL is achieving convergence of the residuals to values less than the residual threshold between plots. However, Table 9 shows that COMSOL is not converging to a solution as the mesh becomes finer because the difference from coarse to normal is 0.28% and the difference from normal to fine is 3.4%. Therefore, the difference between the 2 refinements for each case has increased by a factor of 12 as the mesh is refined. As a result, the solution is diverging rather than converging.

Section VIII: Conclusions and Observations

1. COMSOL was unable to calculate the correct mass flow for t/D ratios ranging between 2 and 8 at a constant critical pressure ratio.
2. COMSOL varied the mass flow rate as a function of pressure ratio—which is incorrect.
3. COMSOL was unable to predict the thermodynamic behavior of the gas in the downstream receiving vessel.
4. The COMSOL calculations for the critical flow cases did not converged—as demonstrated by the grid convergence study.
5. The above all demonstrate that COMSOL is unable to do this problem.
6. The results were not what it was expected. However, this thesis study was able to determine COMSOL's strengths and limitations in the area of critical gas flow through choked orifices and downstream conditions. COMSOL Multiphysics is a friendly CFD software, and a popular tool in the industry, therefore a study of this kind will be useful for future studies.

References

- Deckker, B. E. L., and Chang, Y.F., 1965-66, *An investigation of steady compressible flow of air through square edged orifices*, Proc. Instn. Mech. Engrs., 180, (Pt. 3J), 312-323
- Barthel, H.O., 1957, *On a mechanism for the interaction of plane traveling shock waves striking rigid grid-like structures head-on*, In: Fifth Midwestern Conference of Fluid Mech, University Michigan, USA.
- Brain, T. J. S., and J. Reid, 1975, *Performance of small diameter cylindrical critical flow nozzles*, National Engineering Laboratory Report 546.
- COMSOL, 2017, *Introduction to COMSOL Multiphysics, version 5.3*, COMSOL, Inc.
- Dosanjh, D.S., 1956, *Interaction of grids with traveling shock waves*, NACA TN 3680.
- Franks, W.J., 1957, *Interaction of a shock wave with a wire screen*, UTIA Tech. Note No. 13.
- Frei, W., 2017, *Which Turbulence Model Should I Choose for My CFD Application?*, COMSOL, Inc.
- Frei, W., 2013, *Meshing Considerations for Linear Static Problems*, COMSOL, Inc.
- Grace, H.P., and Lapple, C. E., 1951, *Discharge coefficients of small diameter orifices and flow nozzles*, Trans. Am. Soc. Mech. Engrs., 73, 639-647
- Husain Z., 1995, *Theoretical uncertainty of orifice flow measurement*, Daniel Flow Products, Inc.
- Jackson, R. A., 1963, *The compressible discharge of air through small thick plate orifices*, Appl. Scient. Res., Section A, 13, 241-248 62

Kastner, L. J., Williams, T.J., and Sowden, R. A., 1964, *Critical-flow nozzle meter and its application to the measurement of mass flow rate in steady and pulsating streams of gas*, J.

Maestas, J., 2015, *Flow measurement using critical flow orifices: A Study of Their Limitations and Strengths*, M.S. thesis, Idaho State University.

Miller, R.W., 1983, *Flow Measurement Engineering Handbook*, McGraw-Hill Co, page 13-4, equation 13.9, page 13-25, equation 13.23, page 13-26, equation 13.24.

Perry, J. A., 1949, *Critical Flow Through Sharp-edged Orifices*, Trans. A.S.M.E., vol. 71, p. 757.

Rohde, J. E., Richards, H. T., and Metger, G. W., 1969, *Discharge coefficients for thick plate orifices with approach flow perpendicular and inclined to the orifice axis*, National Aeronautics and Space Administration NANA TN D-5467.

Sharipov, F., 1998, *Data on Internal Rarefied Gas Flows*, Journal of Physical and Chemical Reference Data 27, 657.

Ward, A. & Smith., J. 1979, *Critical Flowmetering: The Characteristics of Cylindrical Nozzles with Sharp Upstream Edges*. International Journal of Heat and Fluid Flow, Vol: 1, pp. 123-132.

Appendices

Appendix A: Knudsen number calculation

$\lambda = 5.9\text{E-}1$ m (vacuum conditions)

$L = 1/16\text{-inch} = 0.0015875$ m

$$Kn = \frac{\lambda}{L}$$

$Kn = 372.3$

$Kn > 0.01 \rightarrow$ Rarified gas

Appendix B: COMSOL study procedure

Procedure for a High Mach Number Flow k- ϵ study:

- 1) New
 - a. In the New window, click Model Wizard
- 2) Model Wizard
 - a. In the select space dimension, click 2D.
 - b. In the select physics tree, select Fluid Flow>High Mach Number Flow>Turbulent Flow>High Mach Number Flow, k- ϵ (hmnf).
 - c. Click Add.
 - d. Click Study
 - e. In the select study tree, select Preset Studies for Selected Physics Interfaces>Stationary.
 - f. Click Done.
- 3) Global Definitions
 - a. Right click on Global definitions
 - b. On the Global Definitions toolbar, click Parameters
 - c. In the Parameters window, enter the data described in Figure 21. Since three orifice sizes are to be studied, the value of “do” is changed for each orifice study case.

Settings			
Parameters			
Parameters			
Name	Expression	Value	Description
Le	3.5[in]	0.0889 m	Entrance line
t	0.125[in]	0.003175 m	Orifice thickness
Lp	2[in]	0.0508 m	Orifice to Tank length
Lt	50.2[cm]	0.502 m	Tank height
de	0.43[in]	0.010922 m	Entrance diameter
do	(1/16)[in]	0.0015875 m	Orifice diameter
dp	0.62[in]	0.015748 m	Orifice to Tank diameter
dt	25.59[cm]	0.2559 m	Tank diameter
Rgas	296[J/kg/K]	296 J/(kg·K)	Gas constant
Area	$0.25 \cdot \pi \cdot do \cdot do$	$1.9793E-6 \text{ m}^2$	Area of orifice
gam	1.4	1.4	Ratio of specific heats

Figure 21. Parameters.

4) Geometry

- a. On the Geometry 1 toolbar, click rectangle.
- b. Repeat step 4.a three more times.
- c. Rectangles
 - i. Rectangle 1 (entrance line)
 - A. In the Width field, type de.
 - B. In the Height field, type Le.
 - C. In the x field, type 0 m.
 - D. In the y field, type 0 m.
 - E. Click Build Selected.
 - ii. Rectangle 2 (orifice)

- A. In the Width field, type d_o .
 - B. In the Height field, type t .
 - C. In the x field, type $d_e/2 - d_o/2$.
 - D. In the y field, type $-t$.
 - E. Click Build Selected.
- iii. Rectangle 3 (downstream)
 - A. In the Width field, type d_p .
 - B. In the Height field, type L_p .
 - C. In the x field, type $d_e/2 - d_p/2$.
 - D. In the y field, type $-t - L_p$.
 - E. Click Build Selected
- iv. Rectangle 4 (Receiving tank)
 - A. In the Width field, type d_t .
 - B. In the Height field, type L_t .
 - C. In the x field, type $d_e/2 - d_t/2$.
 - D. In the y field $-t - L_p - L_t$.
 - E. Click Build Selected.
- i. Union 1 (*uni 1*)
 - A. On the Geometry 1 toolbar, click Booleans and Partitions>Union.
 - B. On the Union settings window, select all four domains (r1, r2, r3, r4).

5) Materials

- a. On the Global Definitions>Materials toolbar, click Add Material.
- b. On the Add Material window, type nitrogen.

- c. On the Add Material tree, select Liquid and Gases>Gases>Nitrogen.
 - d. On the Component 1>Materials>Nitrogen [gas], select all four domains.
- 6) High Mach Number Flow, k- ϵ : On the toolbar, click Initial Values, Inlet, and Outlet
- a. High Mach Number Flow, k- ϵ (hmnf)
 - i. On the Ambient absolute pressure, type “12.5[psi]”
 - b. Fluid 1.
 - i. On the Gas constant type, select Specific gas constant.
 - ii. On the specific gas constant list, select User defined. Type “296”
 - iii. On the Specify Cp or γ list. Select Ratio of specific heats. Type 1.4.
 - c. Wall 1.
 - i. On Boundary conditions list, select Wall functions.
 - ii. Check Apply wall roughness box.
 - iii. On roughness model list, select sand roughness.
 - iv. On equivalent sand roughness height type “0.002[mm]”.
 - d. Initial values 1
 - i. On the velocity y field, type “-348” (speed of sound for nitrogen) since a choked velocity is expected at the orifice.
 - ii. On the pressure field, type “12.5[psi]”.
 - iii. On the temperature field, type “292.7”.
 - e. Initial values 2
 - i. On the Domain Selection, select domain 1.
 - ii. On the pressure field, type “0.86[psi]”.
 - iii. On the temperature field, type “291.4”.

f. Inlet 1

- i. On the Boundary Selection, select boundary 9 as seen in Figure 22.
- ii. On the input state list, select Total.
- iii. On Total pressure field, type “31.24[psi]”.
- iv. On Total temperature field, type “292.7”.
- v. On Mach number field, type “0.002”. (Initial ~ zero velocity is assumed)
- vi. On the Turbulent length scale, type “0.07*de”

g. Outlet 1

- i. On Boundary Selection, Select boundary 2 as seen in Figure 22.
- ii. On the Flow conditions list, select Subsonic.
- iii. On the Boundary condition list, select Pressure.
- iv. On the Pressure field, type “16.48[psi]”.

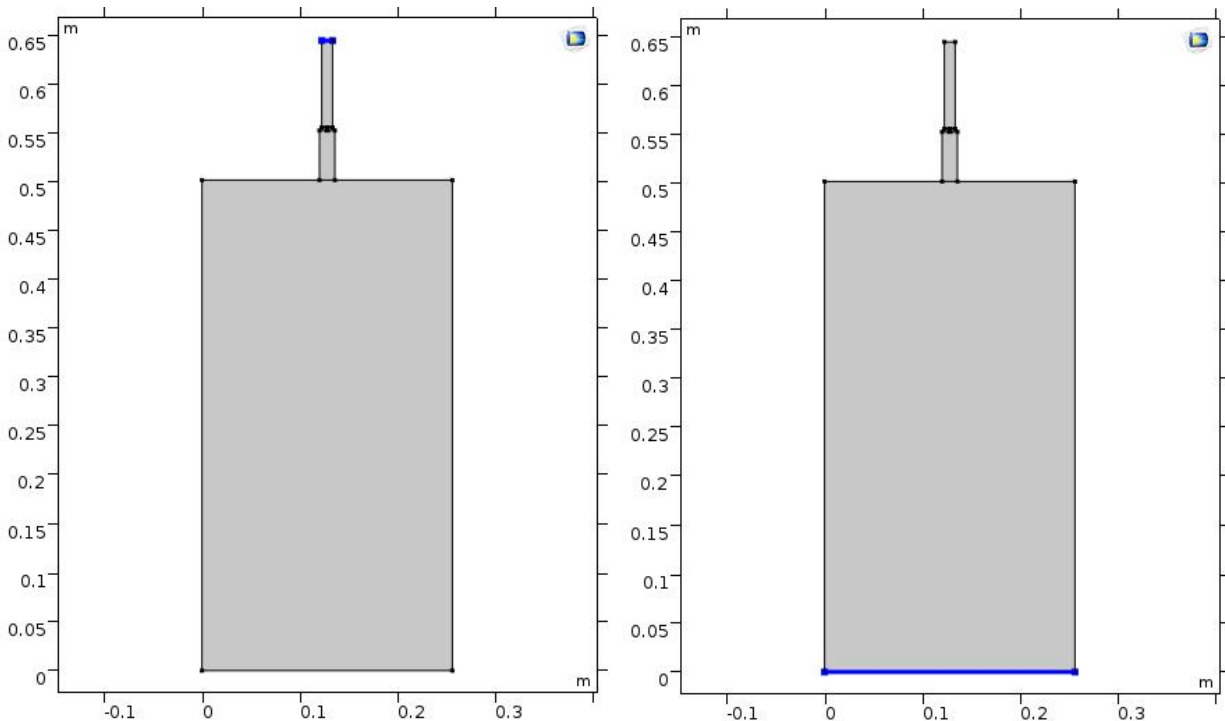


Figure 22. Inlet (left) and Outlet (right) boundaries.

7) Mesh 1

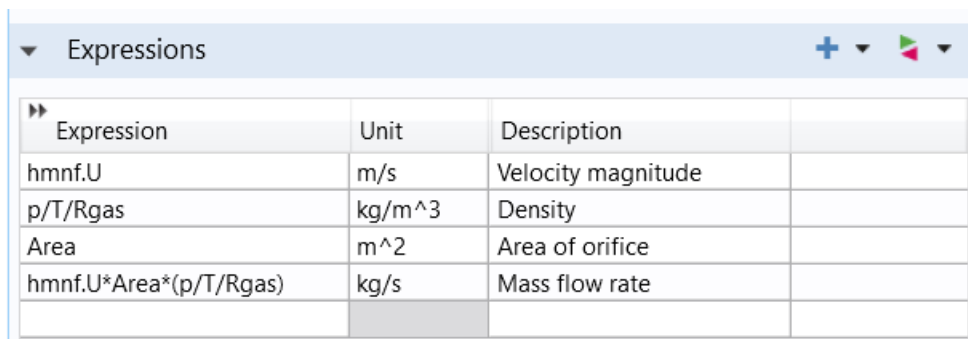
- a. On Sequence type, choose Physics-controlled mesh.
- b. On Element size, choose Coarse.

8) Study

- a. On Step 1: Stationary, click compute.

9) Results

- a. On the Derived Values toolbar, select Average>Surface Average.
- b. On Surface Average, select the orifice or domain 4.
- c. On the Expression field, type what Figure 23 describes to calculate the critical mass flow rate.
- d. Hit compute.



Expressions			
Expression	Unit	Description	
hmnf.U	m/s	Velocity magnitude	
p/T/Rgas	kg/m^3	Density	
Area	m^2	Area of orifice	
hmnf.U*Area*(p/T/Rgas)	kg/s	Mass flow rate	

Figure 23. Average surface derivation expressions for a receiving vessel model.

Appendix C: Mass flow rate calculations

HMNF k-ε, 1/16-inch:

hmnf.U=389.98[m/s] (average velocity at the orifice)

P= 120,960[Pa] (Average pressure at the orifice)

T= 314.9[K] (Average Temperature at the orifice)

R= 296 [J/kg/K] (Gas constant)

P/T/Rgas= 1.3028 [kg/m³] (average density at the orifice)

Area=1.979E-6[m²] (Cross-sectional area of the orifice)

Hmnf.U*(P/T/Rgas)*Area= 7.4016E-4[kg/s] (Mass flow rate)

HMNF k-ε, 1/32-inch:

hmnf.U= 311.47[m/s] (average velocity at the orifice)

P= 124,770 [Pa] (Average pressure at the orifice)

T= 311.47 [K] (Average Temperature at the orifice)

R= 296 [J/kg/K] (Gas constant)

p/T/Rgas=1.4105 [kg/m³] (average density at the orifice)

Area=4.9483E-7[m²] (Cross-sectional area of the orifice)

Hmnf.U*(P/T/Rgas)*Area=2.1523E-4[kg/s] (Mass flow rate)

HMNF k-ε, 1/64-inch:

hmnf.U=308.78[m/s] (average velocity at the orifice)

P= 131,020[Pa] (Average pressure at the orifice)

T= 294.20[K] (Average Temperature at the orifice)

R= 296 [J/kg/K] (Gas constant)

p/T/Rgas=1.31[kg/m³] (average density at the orifice)

Area=1.237E-7[m²] (Cross-sectional area of the orifice)

Hmnf.U*(P/T/Rgas)*Area=5.7003E-5[kg/s] (Mass flow rate)

Appendix D: COMSOL convergence plots

Hmnf k- ϵ cases:

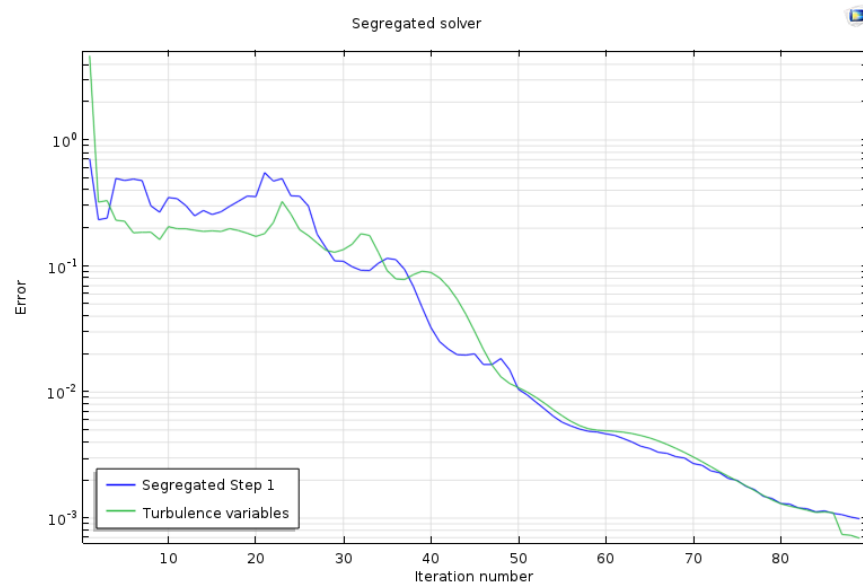


Figure 24. 1/16-inch convergence plot (hmnf k- ϵ).

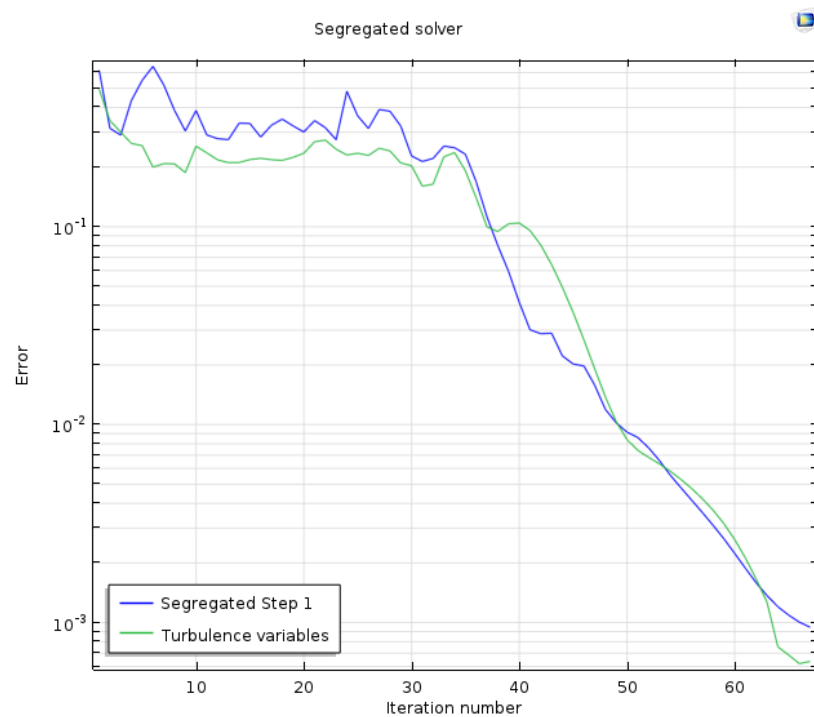


Figure 25. 1/32-inch convergence plot (hmnf k- ϵ).

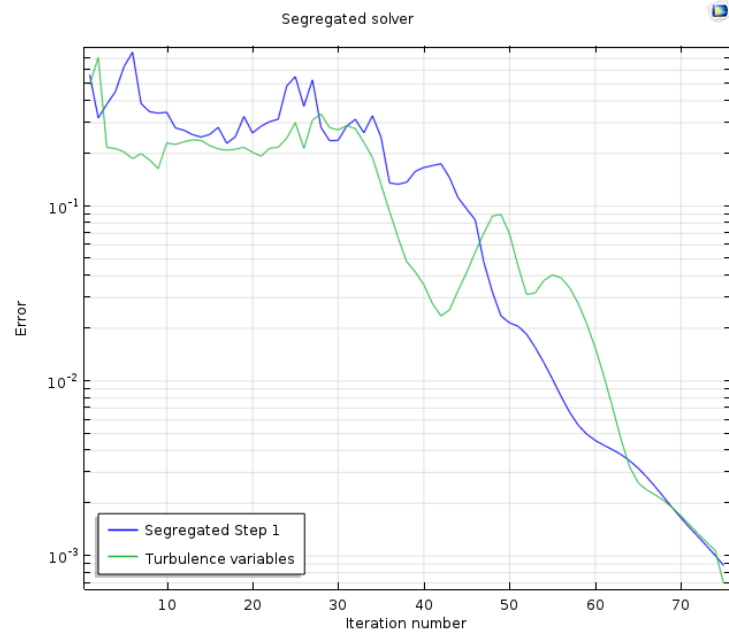


Figure 26. 1/64-inch convergence plot (hmnf $k-\epsilon$).

Appendix E: Maestas results

Table 10. Maestas average mass flow rates.

Orifice Plate	Measure Flow Rate				Theoretical Equations							
	Ideal Gas				Zucker				Spink			
1/16-inch	6.235	+/-	0.2824	lbm/hr	6.669	+/-	0.0984	lbm/hr	6.494	+/-	0.3308	lbm/hr
1/32-inch	1.765	+/-	0.2698	lbm/hr	1.661	+/-	0.0346	lbm/hr	1.500	+/-	0.1593	lbm/hr
1/64-inch Regular	0.399	+/-	0.2733	lbm/hr	0.431	+/-	0.0124	lbm/hr	0.393	+/-	0.0670	lbm/hr
1/64-inch Chamfered	0.495	+/-	0.2706	lbm/hr	0.456	+/-	0.0131	lbm/hr	0.415	+/-	0.0708	lbm/hr